THE JOURNAL OF PHYSICAL CHEMISTRY B

Article

pubs.acs.org/JPCB

Electrohydrodynamic Flow through a 1 mm^2 Cross-Section Pore Placed in an Ion-Exchange Membrane

Kentaro Doi,* Ayako Yano, and Satoyuki Kawano*

Department of Mechanical Science and Bioengineering, Graduate School of Engineering Science, Osaka University, Toyonaka, Osaka 560-8531, Japan

ABSTRACT: In recent years, the control of ionic currents has come to be recognized as one of the most important issues related to the efficient transport of single molecules and microparticles in aqueous solutions. However, the complicated liquid flows that are usually induced by applying electric potentials have made it difficult to address a number of unsolved problems in this area. In particular, the nonequilibrium phenomena that occur in electrically non-neutral fields must be more thoroughly understood. Herein, we report on the development of a theoretical model of liquid flows resulting from ion interactions while focusing on the so-called electrohydrodynamic (EHD) flow. We also discuss the development of an experimental system to optically and electrically observe EHD flows using a 1 mm^2 cross-section pore placed in an ion-exchange membrane where cation and anion flows can be separated without the use of a charged environment. Although micro/nanosized flow channels are usually applied to induce electric double layer overlaps to utilize strong electroosmotic effects, our system does not require such laborious fabrication processes. Instead, we visualize EHD flows by using a millimeter size pore immersed in an alkaline aqueous solution. In this setup, liquid flows passing through the pore along the direction of ion flow, whose velocity reaches on the order of 1 mm/s, can be clearly observed by applying a few volts of electric potential. Furthermore, the transient phenomena associated with ionic responses are theoretically elucidated.

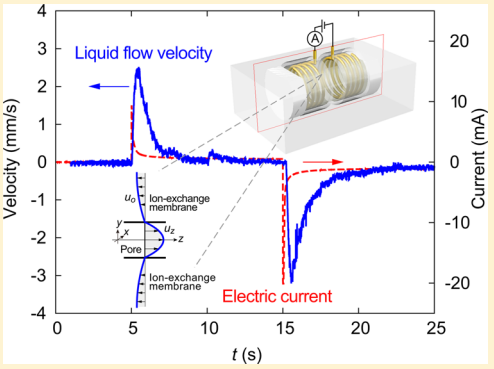

INTRODUCTION

In recent decades, the use of micro/nanofluidic devices in the creation of novel bionanotechnologies has attracted significant attention. As a result, a number of cutting-edge devices, such as the electrochemical capacitor,[1−5] the ion electric field transistor,[6−10] and the single molecule sequencer,[11−18] have been developed. In these technologies, the behavior of electrolyte ions plays an important role in improving output efficiencies. In an aqueous solution, electrolyte ions are exposed to externally applied fields. In particular, ions or electrically charged particles are driven by the electric force known as electrophoresis,[19−22] and liquid flows induced by surface charges on a wall are known as electroosmotic flow (EOF).[20,21,23,24] In micro/nanofluidic devices, electrolyte solutions are strongly polarized in an electric double layer (EDL) near a channel wall, which cause EOF parallel to the wall surface. To induce strong flow fields, finely tuned conditions are satisfied, such as ensuring that the facing walls are less than a few tens of nanometers apart, and that salt concentrations are kept less than 1 mM.[20,21] In conventional models, it is believed that positive and negative ions are usually paired. Therefore, such solutions are considered to be electrically neutral everywhere except near the electrically charged surfaces.[25] More specifically, oppositely signed ions are usually equilibrated in solution because even a modest elongation of an equilibrium length between two ions results in a strong Coulomb force that causes them to attract each other. Accordingly, further understanding will be necessary for future progress.

Electrohydrodynamics was first explored in the pioneering works of Melcher and Taylor[26] and Saville.[27] Additionally, an assembly of polystyrene particles enhanced by electrohydrodynamic (EHD) flows was experimentally observed by Trau et al.[28,29] and numerically analyzed by Ristenpart et al.[30] Furthermore, EHD micropumping applications[31,32] and EHD flow variations[33,34] were reported in some literature reports. Essentially, EHD flows are based on external electric force applied to liquid flows, where an electric potential expressed by the Poisson equation plays an external force in the Navier−Stokes equation. In actual systems, EHD flow observations are only possible in highly polarized conditions such as those shown in EDL[28,29,32] and in the strong electric fields required to apply at least several tens of volts of electric potential.[31,32] EOF is particularly effective on flows near EDL and is, therefore, often combined with EHD. This means that it is difficult to detect EOF separately from electrically charged surfaces in bulk solutions due to the electroneutrality factor, as mentioned above.[25]

Because we are also interested in ion transports in various spatial scales,[22,35−37] in this study, we investigate EHD flows in

Received: July 17, 2014
Revised: November 18, 2014

dx.doi.org/10.1021/jp5071538 | J. Phys. Chem. B XXXX, XXX, XXX−XXX

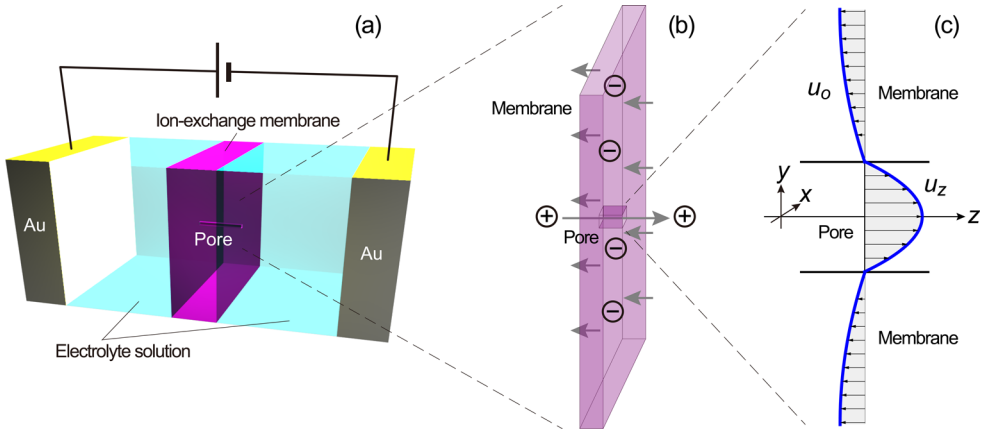

Figure 1. Theoretical model. (a) An ion-exchange membrane in which a small pore is placed is immersed in an electrolyte solution and then exposed to external electric fields. (b) When an anion-exchange membrane is immersed in an alkaline solution, anions can pass through the entire face, whereas cation penetration is limited to the pore. (c) In such ion transport situations, EHD flows will be induced separately in both the membrane and pore.

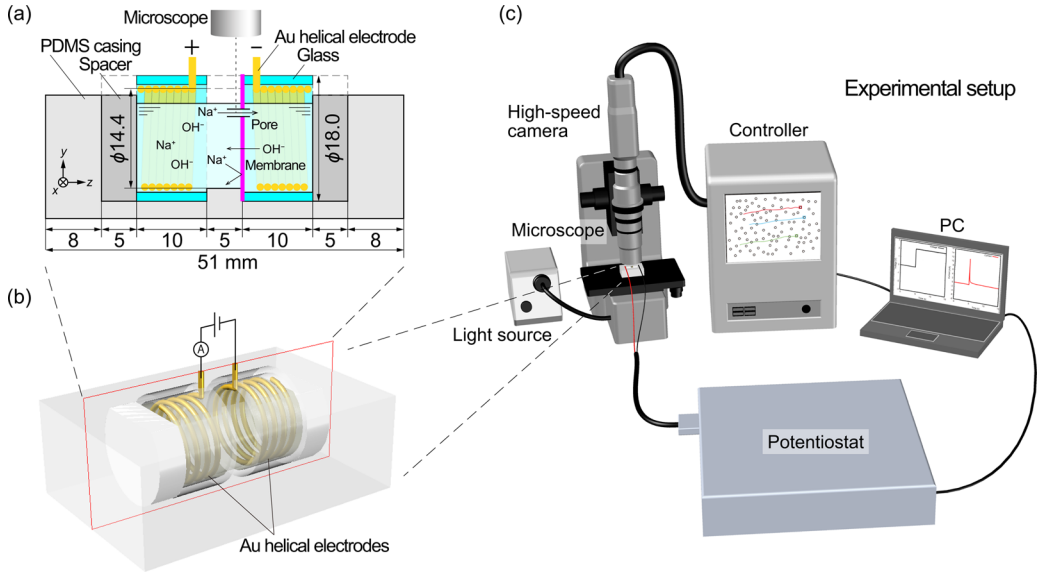

Figure 2. Schematic illustrations of experimental setup: (a) cross-sectional view, (b) 3D view of the present device, and (c) complete overview, where liquid flows are optically observed using a microscope equipped with a high-speed camera and are electrically measured using a potentiostat.

aqueous solutions, while proposing a novel method that does not require any difficult fabrication processes. Specifically, a 1 mm^2 cross-section pore is made in an ion-exchange membrane that has a cross-sectional area large enough to negate the effect of surface charges (Figure 1). Then water flow driven by ionic motions is observed by using a microscope and a high-speed camera. Using this experimental system, it is possible to use the membrane pore to separate the current paths of negative and positive ions (Figure 2). Short-duration nonequilibrium responses just after applying an electric potential can be detected by applying a few volts of electric potential in an aqueous solution corresponding to an electric field on the order of 100 V/m. It should be noted that highly tuned techniques and time-consuming processes are not needed to prepare such a device. After the response, the liquid flow seems to equilibrate to a steady current condition. This finding means that an electrically polarized condition can be induced at an area far from the electrode surfaces. That is, the breakdown of electroneutrality in bulk solutions is achieved. Furthermore, the time and spatial scales of the phenomenon can be well explained by a theoretical EHD flow model.

THEORETICAL MODEL OF AN EHD FLOW THROUGH A PORE

In this section, we show the development of a theoretical model for EHD flow through ion-exchange membranes. First, incompressible liquid flow, which is driven by electric fields, is expressed by the Navier–Stokes equations:

$$\rho_m\left(\frac{\partial}{\partial t} + \mathbf{u}\cdot\nabla\right)\mathbf{u} = -\nabla p + \mu\Delta\mathbf{u} + \sum_i \rho_i\mathbf{E} \quad (1)$$

$$\nabla\cdot\mathbf{u} = 0 \quad (2)$$

where ρ_m is the mass density, $\mathbf{u}(\mathbf{r},t)$ is the velocity, μ is the viscosity, $p(\mathbf{r},t)$ is the pressure, $\mathbf{E}(\mathbf{r},t)$ is the electric field, and $\rho_i(\mathbf{r},t)$ is the electric charge density of the ith species. In electrolyte solutions, ion behavior is described by the Nernst–Planck equation:

dx.doi.org/10.1021/jp5071538 | J. Phys. Chem. B XXXX, XXX, XXX–XXX

$$\frac{\partial \rho_i}{\partial t} = -\nabla \cdot \mathbf{j}_i \tag{3}$$

$$\mathbf{j}_i = \left(\frac{z_i e \mathbf{E}}{\zeta_i} - D_i \nabla + \mathbf{u} \right) \rho_i \tag{4}$$

where z_i is the valence number, e is the elementary charge, ζ_i is the friction coefficient, and D_i is the diffusion coefficient. The electric fields and electric current density obey the Maxwell equations:

$$\varepsilon \varepsilon_0 \nabla \cdot \mathbf{E} = \sum_i \rho_i \tag{5}$$

$$\mathbf{j} = \sum_i \mathbf{j}_i + \varepsilon \varepsilon_0 \frac{\partial \mathbf{E}}{\partial t} \tag{6}$$

$$\nabla \cdot \mathbf{j} = 0 \tag{7}$$

where ε and ε_0 are the relative dielectric constant and dielectric constant of vacuum. By substituting eqs 5 and 6 into eq 7, eqs 3 and 4 are found to be satisfied. That is, ionic currents in electrolyte solutions satisfy the Maxwell equations. When variables are nondimensionalized as follows:

$$\mathbf{r}^* = \frac{\mathbf{r}}{L}, \quad \mathbf{u}^* = \frac{\mathbf{u}}{U}, \quad t^* = \frac{Ut}{L}, \quad \rho_i^* = \frac{L\rho_i}{\varepsilon_0 E_0},$$
$$\mathbf{j}_i^* = \frac{\mathbf{j}_i L^2}{\varepsilon_0 E_0 D_i}, \quad \mathbf{E}^* = \frac{\mathbf{E}}{E_0}, \quad p^* = \frac{p}{\rho_m U^2} \tag{8}$$

where L is the characteristic length, U is the characteristic speed, and E_0 is the uniform electric field, and eqs 1 and 2 are transformed to

$$\left(\frac{\partial}{\partial t^*} + \mathbf{u}^* \cdot \nabla \right) \mathbf{u}^* = -\nabla p^* + \frac{1}{\mathrm{Re}} \Delta \mathbf{u}^* + \xi \sum_i \rho_i^* \mathbf{E}^* \tag{9}$$

$$\nabla \cdot \mathbf{u}^* = 0 \tag{10}$$

where $\xi = \varepsilon_0 E_0^2 / (\rho_m U^2)$ and Re is the Reynolds number. Equations 3 and 4 become

$$\frac{\partial \rho_i^*}{\partial t^*} = -\frac{1}{\alpha_i \mathrm{Pe}} \nabla \cdot \mathbf{j}_i^* \tag{11}$$

$$\mathbf{j}_i^* = (\eta_i^* \mathbf{E}^* - \nabla + \alpha_i \mathrm{Pe} \mathbf{u}^*) \rho_i^* \tag{12}$$

where we focus on a diffusion coefficient D_m of mainly effective species and set $\alpha_i = D_m/D_i$, and then the Péclet number is defined as $\mathrm{Pe} = LU/D_m$. Additionally, the dimensionless mobility is defined as $\eta_i^* = z_i e E_0 L / \zeta_i D_i$. Furthermore, eqs 5−7 result in

$$\varepsilon \nabla \cdot \mathbf{E}^* = \sum_i \rho_i^* \tag{13}$$

$$\mathbf{j}^* = \sum_i \frac{1}{\alpha_i \mathrm{Pe}} \mathbf{j}_i^* + \varepsilon \frac{\partial \mathbf{E}^*}{\partial t^*} \tag{14}$$

$$\nabla \cdot \mathbf{j}^* = 0 \tag{15}$$

Hereafter, we will omit the asterisk symbol for nondimensionalization. According to the schematic illustration in Figure 1, we assume that the velocity field is dominant along the pore axis (z-axis) such that $\mathbf{u} = (0,0,u_z)$. The velocity field is constant along the z-axis, and thus u_z is independent of z such that $u_z = u_z(x,y,t)$, where $(x,y) \in [0,1] \times [0,1]$ for a square cross-section and $t \in [0,\infty)$. As mentioned above, the driving force of the liquid depends on the charge difference of electrolyte ions within a short period, as described by eqs 11 and 12, where the ionic current response consists of electrophoresis, diffusion, and convection. The relationship between the electric charge density and electric field is given by the Poisson equation (eq 13), and thus the electric field depends on ion behavior.

According to the numerical results of the coupled Nernst−Planck and Poisson equations provided in a previous study,[22] the nonuniformity of electric fields is apparent near electrodes, and weak uniform fields remain in solution at points farther away from the electrodes. In our experimental setup, the flow channel is sufficiently separated from both electrodes to allow the electric fields in the pore to be potentially approximated as uniform along the z-axis. Associated with the numerical solution, we replace the dimensionless electric force in eq 9 by

$$\sum_i \rho_i(z,t) E(z,t) \equiv \rho(z,t) E(z,t) \approx \sum_j f_j \exp(-\lambda_j t) \tag{16}$$

The force field is represented by exponents with the amplitude f_j and time scale λ_j, where these constants are determined from experimental results. As usual, it is known that the EHD flows are proportional to the square of the electric field strengths.[32] In our model, the electric force is also proportional to E_0^2 insofar as $\sum_i \rho_i$ and E are uniform in eq 9. On the other hand, in actual systems, concentrations and electric fields tend to deviate from uniformity very near the electrodes, causing them to screen the surface charges. When the upper surface of the liquid is fully exposed to air and the pressure gradient is assured to be negligibly small compared to the electric force term, eqs 9 and 10 are replaced by

$$\frac{\partial u_z}{\partial t} = \frac{1}{\mathrm{Re}} \Delta u_z + \xi \sum_j f_j \exp(-\lambda_j t) \text{ in pore} \tag{17}$$

$$\frac{\partial u_o}{\partial t} = \frac{1}{\mathrm{Re}} \Delta u_o + \xi \sum_j f_j' \exp(-\lambda_j' t) \text{ in membrane} \tag{18}$$

where Re is assumed to be the same in both regions. Due to the continuity of liquid flow, eqs 17 and 18 should satisfy

$$\int_S u_z \mathrm{d}x\mathrm{d}y + \int_{S'} u_o \mathrm{d}x\mathrm{d}y = 0 \tag{19}$$

For nonslip boundary conditions in the pore and an initial condition:

$$u_z(0,y,t) = u_z(1,y,t) = 0 \tag{20}$$

$$u_z(x,0,t) = u_z(x,1,t) = 0 \tag{21}$$

$$u_z(x,y,0) = 0 \tag{22}$$

Solving eq 17, we obtain

$$u_z(x,y,t) = -\frac{16\xi}{\pi^2} \sum_{n_x} \sum_{n_y} \sum_i \frac{f_i}{n_x n_y} \times \frac{\exp(-\lambda_i t) - \exp(-\lambda_k t)}{\lambda_i - \lambda_k} \sin k_x x \sin k_y y \tag{23}$$

dx.doi.org/10.1021/jp5071538 | J. Phys. Chem. B XXXX, XXX, XXX−XXX

$$k_x = n_x\pi, \quad n_x = 1, 3, 5, \cdots \tag{24}$$

$$k_y = n_y\pi, \quad n_y = 1, 3, 5, \cdots \tag{25}$$

$$\lambda_k = \frac{(n_x^2 + n_y^2)\pi^2}{\mathrm{Re}} \tag{26}$$

where the subscript k depends on n_x and n_y. In the ion-exchange membrane, the reverse flow of counterions is effectively developed in $(x,y) \in [0,l'] \times [0,l']$. For initial and boundary conditions:

$$u_o(0,y,t) = u_o(l',y,t) = 0 \tag{27}$$

$$u_o(x,0,t) = u_o(x,l',t) = 0 \tag{28}$$

$$u_o(x,y,0) = 0 \tag{29}$$

we obtain

$$u_o(x,y,t) = -\frac{16\xi}{\pi^2}\sum_{n_x}\sum_{n_y}\sum_i \frac{f_i'}{n_x n_y} \times \frac{\exp(-\lambda_i' t) - \exp(-\lambda_k' t)}{\lambda_l' - \lambda_k'} \sin k_x' x \sin k_y' y \tag{30}$$

$$k_x' = \frac{n_x\pi}{l'}, \quad n_x = 1, 3, 5, \cdots \tag{31}$$

$$k_y' = \frac{n_y\pi}{l'}, \quad n_y = 1, 3, 5, \cdots \tag{32}$$

$$\lambda_k' = \frac{(n_x^2 + n_y^2)\pi^2}{\mathrm{Re}l'^2} \tag{33}$$

Furthermore, to satisfy eq 19, a relation between f_i and f'_i results in

$$\frac{\sum_{n_x}\sum_{n_y}\sum_i f_i' n_x^{-2} n_y^{-2}(\lambda_i' - \lambda_k')^{-1}[\exp(-\lambda_i' t) - \exp(-\lambda_k' t)]}{\sum_{n_x}\sum_{n_y}\sum_i f_i n_x^{-2} n_y^{-2}(\lambda_i - \lambda_k)^{-1}[\exp(-\lambda_i t) - \exp(-\lambda_k t)]} = -\frac{1}{l'^2} \tag{34}$$

EXPERIMENTAL METHODS

Figure 2 shows schematic illustrations of our experimental setup, in which an ion-exchange membrane with a 1 mm^2 cross-section pore is immersed in a 0.1 M NaOH aqueous solution. Helical-shaped Au electrodes are placed on both sides of the membrane and set at a distance at least 5 mm from each other (Figure 2a,b). To facilitate OH^- and anion exchange, an anion-exchange membrane (Neosepta, Astom Co., Ltd., Tokyo, Japan) is employed. The membrane is about 140 μm thick. The reservoir, which holds different-sized cylindrical chambers, is made of polydimethylsiloxane (PDMS). The cylinder with the anion-exchange membrane fixed at one end is 14.4 mm in diameter and 5 mm in length. Another chamber (18.4 mm in diameter and 15 mm in length) is set outside the one mentioned above into which a glass cylinder (18.0 mm in diameter and 10 mm in length) and a spacer (18.0 mm in diameter and 5 mm in length) are placed, as shown in Figure 2a. A 1 × 1 mm^2 cross-section pore penetrates 3 mm into the PDMS channel and is placed in the anion-exchange membrane. Here we chose a square cross-section to ensure high tracer particle contrast to transmitted light. The surface area of the ion-exchange membrane immersed in the solution is at least 100 times larger than that of the pore. A 0.8 μm sized polystyrene particle (Estapor, Merck KGaA Co., Ltd., Darmstadt, Germany) is employed as a tracer, where 10 volume percent of the polystyrene particles is further diluted to 0.1 volume percent, and 200 μL of it is diffused in 3.6 mL of the NaOH solution. Before measurements, the electrodes are electrically shorted, and the solutions are stirred and left for more than 20 min. After that, the equilibrium condition is confirmed by observing the behavior of tracer particles. When an electric potential is applied to the Au electrodes, the motions of tracer particles are observed using a microscope equipped with a high-speed camera (VW-9000, Keyence Co., Ltd., Osaka, Japan) (Figure 2c). The applied potential difference is absolutely set to 2.2 V to obtain clear electric signals. The measurements are carried out at a constant voltage condition. Motions of the particles are tracked with the high-speed camera at a frame rate of 500 fps. Trajectories are traced, and their velocity is analyzed. Electric signals are simultaneously measured with a sampling rate of 200 Hz by using a potentiostat (VersaSTAT4, Amtek, Inc., Oak Ridge, TN).

RESULTS AND DISCUSSION

Theoretical Analysis of EHD Flow through a Pore in Ion-Exchange Membranes. In this section, we first discuss a case of a single exponential electric signal decay caused by ionic responses. Because ionic response differences are not locally distinguished in the actual system, it is reasonable to set an equivalent response time, $\tau_e = \lambda_e^{-1}$, in the pore and ion-exchange membrane. Thus, eq 34 is expressed as

$$\frac{f_e'}{f_e} = -\frac{1}{l'^2}\frac{\sum_{n_x}\sum_{n_y} n_x^{-2} n_y^{-2}(\lambda_e - \lambda_k)^{-1}[\exp(-\lambda_e t) - \exp(-\lambda_k t)]}{\sum_{n_x}\sum_{n_y} n_x^{-2} n_y^{-2}(\lambda_e - \lambda_k')^{-1}[\exp(-\lambda_e t) - \exp(-\lambda_k' t)]} \tag{35}$$

where the amplitude of the electric signal corresponds to f_e and f_e' for the inside and outside of the pore, respectively. Hereafter, we will discuss the case of $f_e = 1$. Figure 3 shows u_z, u_o, and f_e' analyzed for varieties of λ_e and l' at Re = 0.1, where the velocity evaluated at the center of channel, $x = y = 0.5$, is presented and is normalized by ξ. As shown in Figure 3a, we found that a u_z response strongly depends on λ_e when we set $l' = 1.414$. The liquid response time increases with decreasing λ_e. The relative difference between the time scales of liquid flow and the electric signal affects the result. Due to the continuity of the volume flow rate, the velocity is significantly lower in the ion-exchange membrane than in the pore, as far as $l' > 1$. Figure 3b presents the magnitude of f_e' as a function of time. According to eq 35, f_e' rapidly settles at some steady-state values and converges to l'^{-4} as λ_e decreases. Notably, f_e' deviates from the convergence value as λ_e is close to λ_k and λ_k'. Figure 3c,d shows results for the case of $l' = 3.162$. The flow velocity in the ion-exchange membrane is apparently reduced in comparison with Figure 3a, because the cross-sectional area of the flow channel increases proportionally to l'^2. The asymptotic behavior of f_e' is qualitatively the same as Figure 3b, although there is a quantitative difference associated with l'^{-4}. Figure 4 shows results for the case of Re = 1. An increase in Re reduces both λ_k and λ_k' and results in the slow liquid flow response. As shown in Figure 4a, the initial rise of u_z and u_o takes slightly more time, even though the decay of flow velocities is similar to that in Figure 3. Some maximum peaks can be found in the transient responses. Additionally, the

dx.doi.org/10.1021/jp5071538 | J. Phys. Chem. B XXXX, XXX, XXX−XXX

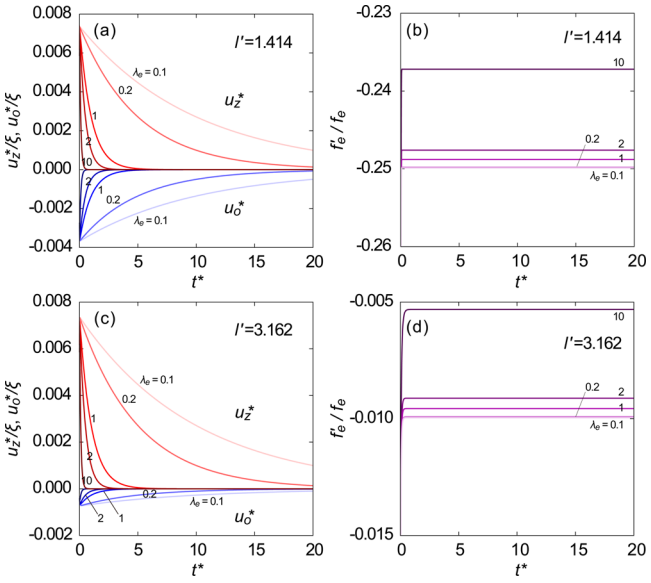

Figure 3. Numerical results of the theoretical model for Re = 0.1: (a) normalized u_z and u_o and (b) f_e'/f_e for $l' = 1.414$; (c) u_z and u_o and (d) f_e'/f_e for $l' = 3.162$. λ_e is varied ranging from 0.1 to 10. u_z and u_o calculated at $(x,y) = (0.5,0.5)$ are presented.

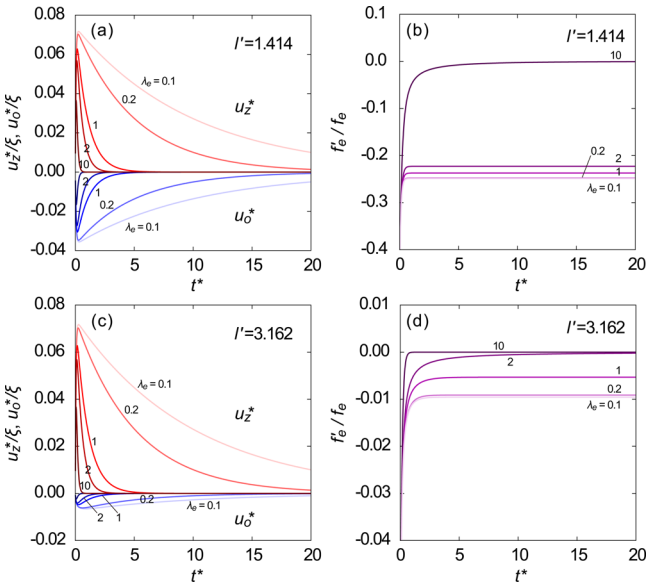

Figure 4. Numerical results of the theoretical model for Re = 1: (a) normalized u_z and u_o and (b) f_e'/f_e for $l' = 1.414$; (c) u_z and u_o and (d) f_e'/f_e for $l' = 3.162$. λ_e is varied ranging from 0.1 to 10. u_z and u_o calculated at $(x,y) = (0.5,0.5)$ are presented.

behavior of f_e' is different from that in Figure 3b. In particular, as shown in Figure 4b, f_e' tends to approach zero when $\lambda_e = 10$. In the case of $l' = 3.162$, u_z and u_o exhibit similar trends with Figure 4a, except for the small amplitude of u_o, as shown in Figure 4c. On the other hand, f_e' tends to deviate from l'^{-4} when $\lambda_e > 1$ and, in particular, approaches zero (Figure 4d). Figure 5 presents results from the case of Re = 10. Initial increases and subsequent decays in the transient responses are clearly found in Figure 5a. In Figure 5b, the response of f_e' also becomes slower and approaches zero when $\lambda_e > 1$. As shown in Figure 5c,d, an increase in l' reduces u_o, and f_e' is clearly modulated by relative differences between λ_e, λ_k, and λ_k'. On the basis of the difference in the surface areas, it is clear that u_z and f_e become

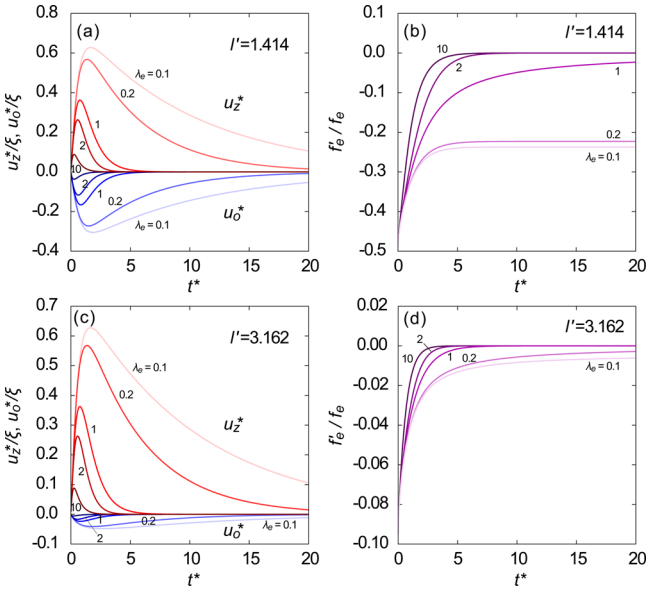

Figure 5. Numerical results of the theoretical model for Re = 10: (a) normalized u_z and u_o and (b) f_e'/f_e for $l' = 1.414$; (c) u_z and u_o and (d) f_e'/f_e for $l' = 3.162$. λ_e is varied ranging from 0.1 to 10. u_z and u_o calculated at $(x,y) = (0.5,0.5)$ are presented.

prominent compared to u_o and f_e', respectively. It has been suggested that the flow field can be magnified relatively in the pore when we design $l' \gg 1$ in actual experimental systems. Figure 6 shows velocity profiles as a function of time along the x-axis at $y = 0.5$ for the case of $\lambda_e = 1$ and $l' = 1.414$. As shown in Figure 6a,b, for small Re, the velocity field develops quickly and decays as a Poiseuille flow. As Re increases in the manner shown in Figure 6c, where the development of velocity fields can be detected, the liquid flow develops almost uniformly during the initial rise and gradually deforms to a Poiseuille flow.

In this section, we discussed an EHD flow that could be realized using a small pore in ion-exchange membranes. It was theoretically demonstrated that temporal EHD flows can be generated if electroneutrality is eliminated by applying electric potentials in electrolyte solutions. Furthermore, it is possible to induce liquid flows associated with the charge difference of ions and electric fields in the pore. As a result, we clarified that the time scale of ionic responses and Re govern the behavior of liquid flows. In the following subsection, we show an experiment performed to confirm that the electroneutrality is actually broken, which then induces an EHD flow.

Visualization and Electrical Observation of EHD Flow. Figure 7 shows current−voltage (IV) characteristics of an anion-exchange membrane with and without a pore. In the present experimental system, the conductance of 0.1 M NaOH solution was electrically measured and resulted in 0.25 mS (Figure 7a). In this solution, the conductance of the pristine membrane was 0.17 mS (Figure 7b) and that of the membrane with a 1 × 1 mm^2 cross-section pore was 0.12 mS (Figure 7c). It was found that the anion-exchange membrane actually became resistant to ionic currents, and that the presence of the pore could not restore equivalent conductance levels. The cross-section area of the PDMS block surrounding the pore possibly blocked the ionic current.

Figure 8 shows electric potential responses that were measured by applying a voltage difference of 2.2 V on the helical-shaped bias electrodes, where the other probe electrodes

dx.doi.org/10.1021/jp5071538 | J. Phys. Chem. B XXXX, XXX, XXX−XXX

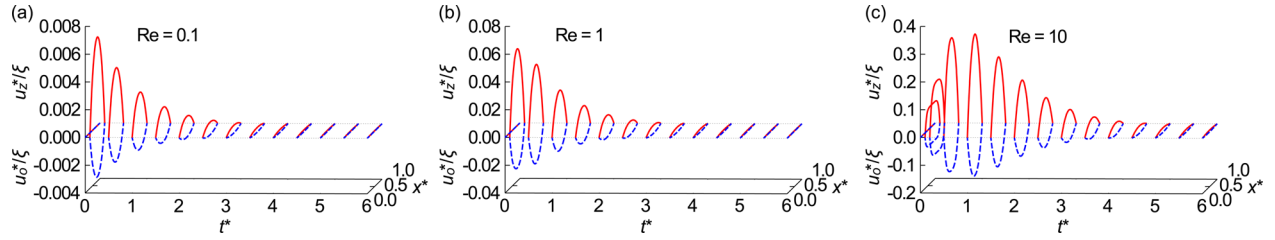

Figure 6. Time evolutions of u_z (solid line) and u_o (dashed line) along the x-axis at $y = 0.5$ for (a) Re = 0.1, (b) Re = 1, and (c) Re =10, where $\lambda_e = 1$ and $l' = 1.414$.

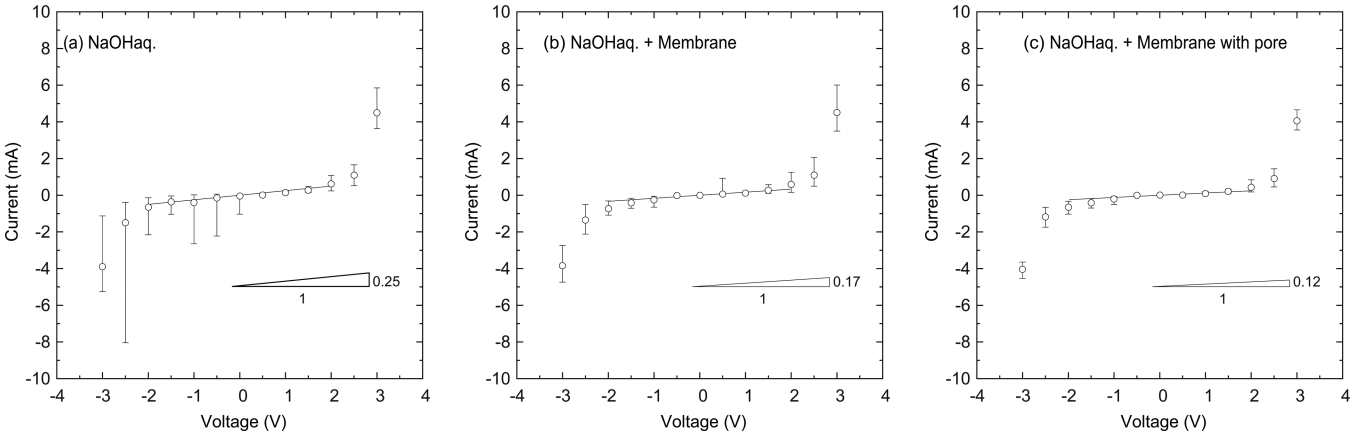

Figure 7. *IV* characteristics measured in the present device for the case of (a) 0.1 M NaOH aqueous solution, (b) a pristine anion-exchange membrane in the NaOH solution, and (c) an anion-exchange membrane with a 1 × 1 mm^2 cross-section pore in the NaOH solution. Error bars indicate minimum and maximum values at each data point, resulting from eight samples in parts a and b and six samples in part c. The conductance is evaluated by linear least-squares fit between −2 and 2 V and results in (a) 0.25 mS, (b) 0.17 mS, and (c) 0.12 mS.

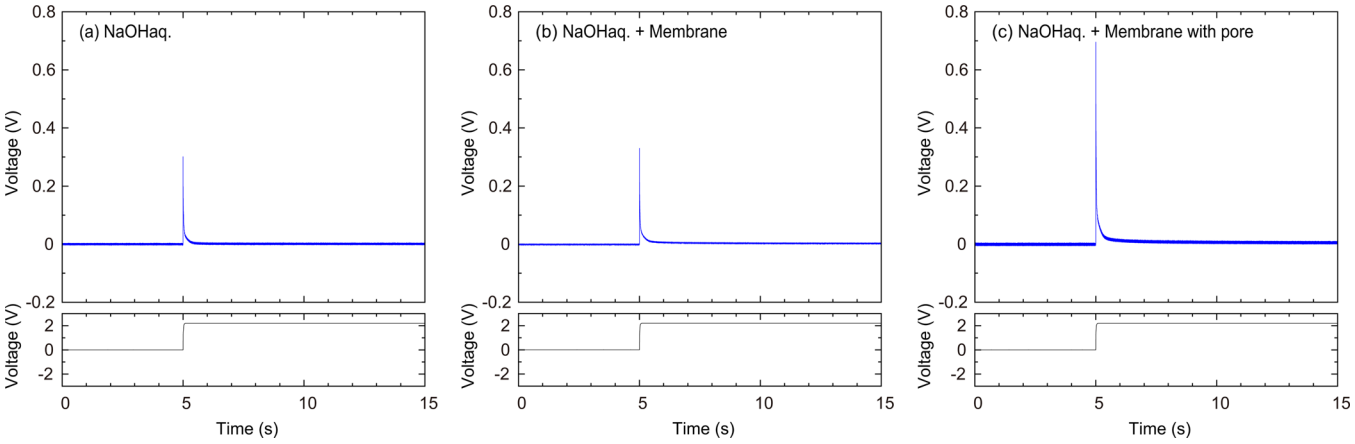

Figure 8. Electric potential response between both ends of membrane when an electric voltage difference of 2.2 V was applied on the helical-shaped bias electrodes in 0.1 M NaOH solution. The other probe was set with the electrode distance of 3 mm (a) without a membrane, (b) across a pristine anion-exchange membrane, and (c) across an anion-exchange membrane with a 1 × 1 mm^2 cross-section pore.

were set across the membrane with the distance of 3 mm between the electrodes. Compared between the transient responses with and without a membrane, a prominent peak was observed by using the membrane with a 1 × 1 mm^2 pore (Figure 8c). It was found that drastic Na^+ concentration changes transiently occurred near the pore immediately after the electric potential was applied, even though this polarization was not maintained at steady states as shown in Figure 7. This trend was also confirmed for the other applied voltages (figures are omitted).

Figure 9 shows some typical transient responses of the liquid flow resulting from the trajectories of tracer particles in the area of 458 × 611 μm^2 ($x \times z$) at the center of the pore, which were independently measured. These results imply that highly concentrated ions in the pore region induce the liquid flow triggered by an applied electric potential. In our experimental system, it was confirmed that electrophoretic transport of the polystyrene particle was not clearly observed in pure water and the NaOH solution, even though the polystyrene particle surfaces were known to have weak negative charges. This means that the electric field strength is too weak to induce electrophoretic particle transport in the bulk condition. Furthermore, in unsteady flows, taking into account the

dx.doi.org/10.1021/jp5071538 | J. Phys. Chem. B XXXX, XXX, XXX−XXX

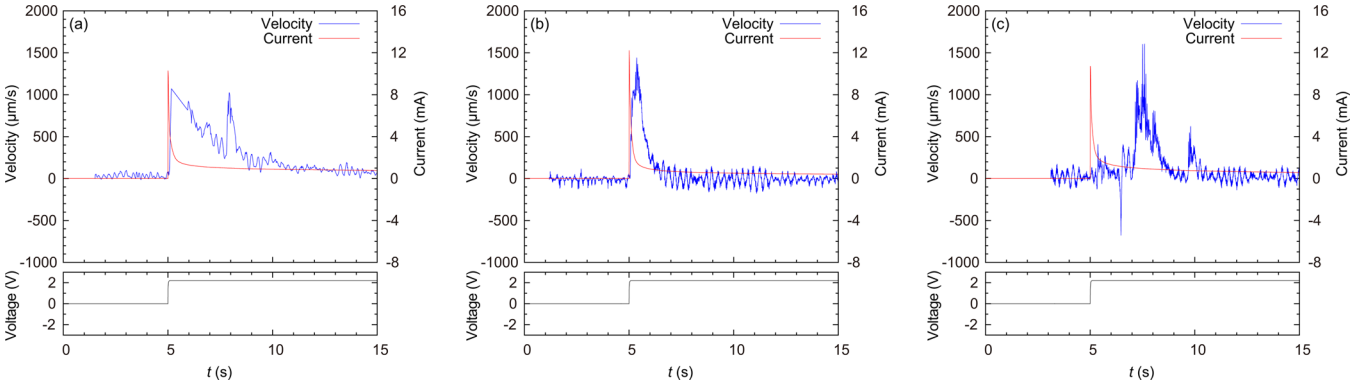

Figure 9. Three typical experimental data of the velocity of liquid flow in the pore and electric current, corresponding to the applied electric potential of 2.2 V at t = 5 s. (a) Following the quick response of electric current, velocity seems to be multiply firing in the decay process. (b) A sharp single spike of the velocity is observed just following the electric signal. (c) After the application of electric potential, an interval of a few seconds occurs until liquid flow is enhanced. Tracer particles were tracked in the area of 458 × 611 μm^2 ($x \times z$) at the center of the pore.

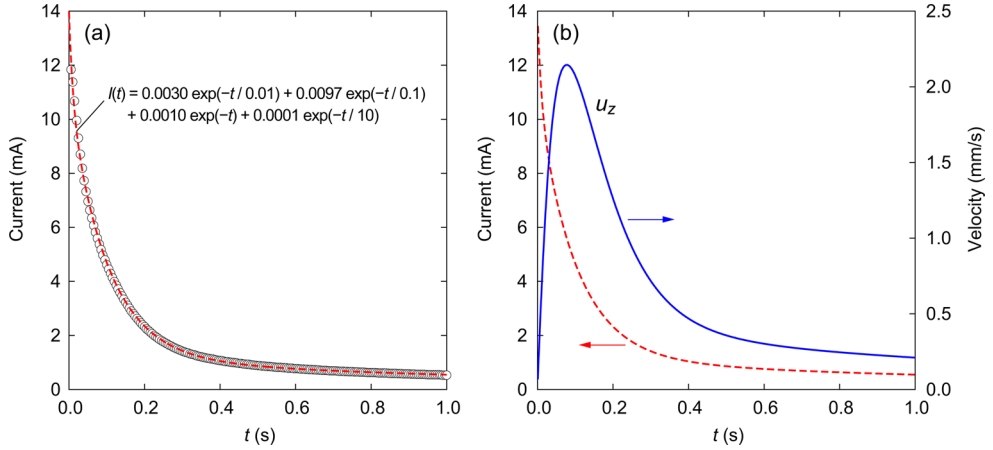

Figure 10. (a) Experimental data (open circle) of electric current response and the least-squares fit (dashed line) by the set of time constants: 0.01, 0.1, 1, and 10 s. (b) Response of u_z (solid line) at $x = y = 0.5$ induced by the electric current response (dashed line) analyzed in (a), where the electric current is translated to the electric force by $I = \beta\rho E$ and $\beta = 2 \times 10^{-4}$ $m^4/(V\ s)$.

additional mass and Basset force, as well as the Stokes drag, particle response time τ_p is approximately expressed as[38−40]

$$\tau_p = \frac{2}{9}\left(\frac{\rho_p}{\rho_m} + \frac{1}{2}\right)\frac{a^2}{\nu} \tag{36}$$

where ρ_p and a are the density and radius of a particle, respectively. In the present case, τ_p is on the order of 1 μs, resulting from $\rho_p/\rho_m \sim 1$, $a \sim 1$ μm, and $\nu \sim 1 \times 10^{-6}$ m^2/s. Such a short response time means that the behavior of particles is fully susceptible to the liquid flow. Actually, the particles simultaneously move in a one-dimensional direction along the z-axis when an electric potential is externally applied. In Figure 9a, an electric potential of 2.2 V was externally applied at t = 5 s, and electric current signal caused by ionic responses was observed immediately thereafter. Following that, liquid flow rate increased and velocity slowly decreased, even though multiple-spike signals seemed to be included in the decay. At the peak point, the liquid flow velocity reached 1 mm/s. Figure 9b also shows a sharp apparent velocity peak, which reached approximately 1.5 mm/s. In this case, the liquid flow response time is shorter than that in Figure 9a. In contrast, Figure 9c showed liquid response retardation, and severe velocity changes were found when the electric current approached a steady condition. Additionally, some peaks could be found in the liquid response. In each case, the particle transport direction was from the positive to negative electrode, which was also the cation flow direction. Furthermore, peculiar oscillations often appeared by applying electric potentials, which was clearly different from the Brownian motion of particles. This phenomenon has not been theoretically explained. Consequently, it is clear that the liquid flow velocity is strongly enhanced by ionic motions in the solution that is recognized via electric signals, even though there are response variations. These experimental results conclude the observation of EHD flow by our system.

The maximum velocity of the peaks was found to reach approximately 1 mm/s. Here, assuming a uniform electric field between the two electrodes, the electric field strength is roughly estimated as ∼100 V/m, which can be evaluated from Figure 8. The liquid velocity field is developed by applying an electric potential and shows continuous decay to zero. Furthermore, even though the electric current signal spike can only be observed for a short period, the liquid flow actually occurs during the following ionic responses. It is, therefore, suspected that an applied electric potential induces ion transport in the electric field, after which a liquid flow is induced in the pore by densely concentrated cations. Although it is believed that ions are usually paired to maintain the electroneutrality of electrolyte solutions, except for externally charged conditions

dx.doi.org/10.1021/jp5071538 | J. Phys. Chem. B XXXX, XXX, XXX−XXX

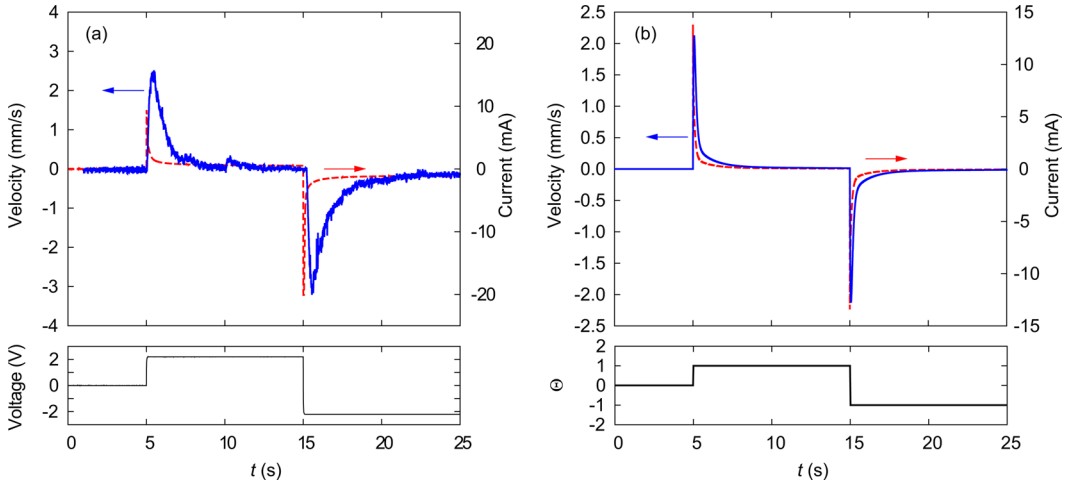

Figure 11. (a) Experimental observation and (b) numerical result of the velocity response (upper panels) to sequential applications of electric potential (lower panels), where the flow velocity and electric current are presented with solid and dashed lines, respectively. The first application of electric potential was at t = 5 s, and the second one was inversely at t = 15 s. In the theoretical model shown in part b, the parameter set employed in Figure 10 was applied.

such as EDL at charged surfaces,[20,25] our results indicate that electroneutrality can be broken without requiring any specific conditions. In our experimental system, the pore was located more than 1 mm away from the electrode. When a pore with a 1 mm^2 square cross-section is filled with water and we apply L = 1 mm and $\nu = 1 \times 10^{-6}$ m^2/s, the time constant of the liquid response is evaluated as $\tau = \lambda^{-1} \approx 0.05$ s from eq 26. This constant appears to be smaller than that of ionic responses measured by electric signals shown in Figure 9. Ionic responses are usually caused by transitions of both ion distributions and electric potentials. Basically, it is a nonlinear response and cannot be determined by a single exponent. This point has already been discussed in a previous study.[22]

As shown in Figure 10a, a measured electric signal was fitted by linear combinations of some exponents considering the time constants of τ_e = 0.01, 0.1, 1, and 10 s. Using these constants, experimental data could be fitted by

$$I(t) = 0.0030 \exp\left(-\frac{t}{0.01}\right) + 0.0097 \exp\left(-\frac{t}{0.1}\right) + 0.0010 \exp(-t) + 0.0001 \exp\left(-\frac{t}{10}\right) \quad (37)$$

In this case, the time constant coefficient of 0.1 s resulted in 0.0097 mA, which was the largest. Additionally, the coefficients of 0.01 and 1 s were also included as factors of 0.003 and 0.001 mA, respectively, and I was sufficiently converged at τ_e = 10 s. Assuming that the ionic current obeys Ohm's law, eq 37 can be related to electric force in eq 23 such that $I = \beta\rho E$, where β is a constant. To represent the experimental data, we set $\beta = 2 \times 10^{-4}$ m^4/(V s). Then ρ is on the order of 1 C m^{-3} for I = 10 mA, which corresponds to the concentration of 1×10^{-8} M for monovalent ions. The results indicate that the charge separation of ions is very weak in actual systems, even if the concentration of NaOH aqueous solution is 0.1 M in equilibrium, which is why electrolyte solutions are usually considered to be close to electroneutral throughout.[25] According to this experimental data fit, the external force can be applied in eq 23, after which the time evolution of u_z produces the results as shown in Figure 10b. These results show that firing an electric spike signal excites the liquid flow and that the successive u_z then shows a maximum peak that slowly decays to zero. Although the contribution of the time constant of 0.1 s may be dominant in eq 37, the response of u_z shows a long tail affected by the other time constants. As shown in Figures 3−5, no single component can explain the characteristics caused by both fast and slow ion responses. That is, ionic responses include various time constants, and the EHD flows are driven as expressed in the theoretical model.

EHD Flow to Sequential Applications of Electric Potentials. Figure 11 shows a velocity response resulting from a sequential application of electric potentials and its theoretical model. When an electric potential of 2.2 V was applied at t = 5 s and −2.2 V was successively applied at t = 15 s, continuous liquid flow responses were clearly observed, as shown in Figure 11a. In the same manner as reported in the previous section, the liquid flow velocity first increased and then showed a slow decay. Furthermore, it also responded to the inversely applied electric potential, and it was found that the EHD flow direction could be reversed sequentially by changing the direction of the electric fields. The mechanism of this phenomenon can be understood using the same model mentioned above. For sequential applications of electric potentials, eq 17 is modified as follows

$$\left[\frac{\partial}{\partial t} - \frac{1}{\mathrm{Re}}\Delta\right]u_z = \xi \sum_i \sum_j f_{ij} \exp[-\lambda_i(t - t_j)]\Theta(t - t_j) \quad (38)$$

where $\Theta(t)$ is the step function. In this case, the solution is

$$u_z(x, y, t) = -\frac{16\xi}{\pi^2} \sum_{n_x} \sum_{n_y} \sum_i \sum_j \frac{f_{ij}}{n_x n_y} \frac{\exp[-\lambda_i(t - t_j)] - \exp[-\lambda_k(t - t_j)]}{\lambda_i - \lambda_k} \Theta(t - t_j) \sin k_x x \sin k_y y \quad (39)$$

dx.doi.org/10.1021/jp5071538 | J. Phys. Chem. B XXXX, XXX, XXX−XXX

This result is presented in Figure 11b. Here we employed the same parameter sets used in Figure 10. Our theoretical model well explains the response trends in the experimental result, where ionic motions enhance liquid flows. More specifically, the inversely applied potentials disturb the steady current state and induce the backward flow of ionic currents. Then the cation flow concentrates at the pore and produces the reverse flow. In the experimental result, the magnitude of the second peak of both the current and the velocity is always larger than the first. The results also show that the environments can be changed slightly for successive electric field applications. When compared to the initial equilibrium condition, the possibility exists that there are differences in the Na^+ concentration on either sides subject to the applied potential. Such differences have not yet been taken into account in the theoretical model. Therefore, the present model does not consider the spatial distribution of ions along the electric fields, although the diffusion of ions along the electric fields takes long periods of time.[22] In this study, we could identify such important points by coupling the electric measurement with optical microscopic observation. To facilitate further improvements, coupling the ion transport processes to the growth process of flow fields should be considered.

CONCLUSION

We succeeded in visualizing an EHD flow induced by a cation flow passing through a 1 mm^2 cross-section pore in an anion-exchange membrane while applying an electric potential of 2.2 V on a 10 mm order length system. Contrary to conventional theories, we found that ion flows could be transiently separated using an EHD flow without applying a charge. In our experimental mechanism, the charge difference was induced due to a pore placed in the membrane by applying electric fields, after which a liquid flow on the order of 1 mm/s was observed until electroneutral conditions were reestablished. We also found that the liquid flow response time scale was affected by ion behavior. Furthermore, it was demonstrated that the liquid flow direction could be changed sequentially via the use of inversely applied electric fields. This observation was also well understood using a theoretical model in which even a small charge difference will cause a strong one-dimensional flow. Considering various ion-exchange membrane and electrolyte solution combinations, this kind of EHD flow is expected to have applications in mass transport, rectification, and liquid flow mixing.

AUTHOR INFORMATION

Corresponding Authors

*E-mail: doi@me.es.osaka-u.ac.jp. Phone: +81 6 6850 6176.
*E-mail: kawano@me.es.osaka-u.ac.jp. Phone: +81 6 6850 6175.

Notes

The authors declare no competing financial interest.

ACKNOWLEDGMENTS

The authors thank Mr. S. Fukazawa for discussions related to the development of the experimental device.

REFERENCES

(1) Conway, B. E. Transition from "Supercapacitor" to "Battery" Behavior in Electrochemical Energy Storage. *J. Electrochem. Soc.* **1991**, *138*, 1539−1548.
(2) Simon, P.; Gogotsi, Y. Materials for Electrochemical Capacitors. *Nat. Mater.* **2008**, *7*, 845−854.
(3) Wei, D.; Scherer, M.; Bower, C.; Andrew, P.; Ryhänen, T.; Steiner, U. A Nanostructured Electrochromic Supercapacitor. *Nano Lett.* **2012**, *12*, 1857−1862.
(4) Xu, Z.; Li, Z.; Holt, C.; Tan, X.; Wang, H.; Amirkhiz, B. S.; Stephenson, T.; Mitlin, D. Electrochemical Supercapacitor Electrodes from Sponge-Like Graphene Nanoarchitectures with Ultrahigh Power Density. *Phys. Chem. Lett.* **2012**, *3*, 2928−2933.
(5) Han, H.; Chong, C.; Wang, S.; Heh, D.; Tseng, C.; Huang, Y.; Chattopadhyay, S.; Chen, K.; Lin, C.; Lee, J.; et al. High K Nanophase Zinc Oxide on Biomimetic Silicon Nanotip Array as Supercapacitors. *Nano Lett.* **2013**, *13*, 1422−1428.
(6) Daiguji, H.; Yang, P.; Majumdar, A. Ion Transport in Nanofluidic Channels. *Nano Lett.* **2004**, *4*, 137−142.
(7) Vlassiouk, I.; Siwy, Z. S. Nanofluidic Diode. *Nano Lett.* **2007**, *7*, 552−556.
(8) Nam, S.; Rooks, M. J.; Kim, K.; Rossnagel, S. M. Ionic Field Effect Transistors with Sub-10 nm Multiple Nanopores. *Nano Lett.* **2009**, *9*, 2044−2048.
(9) Guan, W.; Fan, R.; Reed, M. A. Field-Effect Reconfigurable Nanofluidic Ionic Diodes. *Nat. Commun.* **2011**, *2:506*, 1−8.
(10) Guan, W.; Reed, M. A. Electric Field Modulation of the Membrane Potential in Solid-State Ion Channels. *Nano Lett.* **2012**, *12*, 6441−6447.
(11) Storm, A. J.; Storm, C.; Chen, J.; Zandbergen, H.; Joanny, J.-F.; Dekker, C. Fast DNA Translocation through a Solid-State Nanopore. *Nano Lett.* **2005**, *5*, 1193−1197.
(12) Fologea, D.; Uplinger, J.; Thomas, B.; McNabb, D. S.; Li, J. Slowing DNA Translocation in a Solid-State Nanopore. *Nano Lett.* **2005**, *5*, 1734−1737.
(13) Dekker, C. Solid-State Nanopores. *Nat. Nanotechnol.* **2007**, *2*, 209−215.
(14) Zwolak, M.; Di Ventra, M. Colloquium: Physical Approaches to DNA Sequencing and Detection. *Rev. Mod. Phys.* **2008**, *80*, 141−165.
(15) Branton, D.; Deamer, D. W.; Marziali, A.; Bayley, H.; Benner, S. A.; Butler, T.; Di Ventra, M.; Garaj, S.; Hibbs, A.; Huang, X.; et al. The Potential and Challenges of Nanopore Sequencing. *Nat. Biotechnol.* **2008**, *26*, 1146−1153.
(16) Tsutsui, M.; Taniguchi, M.; Yokota, K.; Kawai, T. Identifying Single Nucleotides by Tunnelling Current. *Nat. Naotechnol.* **2010**, *5*, 286−290.
(17) Venkatesan, B. M.; Bashir, R. Nanopore Sensors for Nucleic Acid Analysis. *Nat. Nanotechnol.* **2011**, *6*, 615−624.
(18) Ohshiro, T.; Matsubara, K.; Tsutsui, M.; Furuhashi, M.; Taniguchi, M.; Kawai, T. Single-Molecule Electrical Random Resequencing of DNA and RNA. *Sci. Rep.* **2012**, *2:501*, 1−7.
(19) Sokalski, T.; Lingenfelter, P.; Lewenstam, A. Numerical Solution of the Coupled Nernst−Planck and Poisson Equations for Liquid Junction and Ion Selective Membrane Potentials. *J. Phys. Chem. B* **2003**, *107*, 2443−2452.
(20) Schoch, R. B.; Han, J.; Renaud, P. Transport Phenomena in Nanofluidics. *Rev. Mod. Phys.* **2008**, *80*, 839−883.
(21) Sparreboom, W.; Berg, A.; Eijkel, J. Principles and Applications of Nanofluidic Transport. *Nat. Nanotechnol.* **2009**, *4*, 713−720.
(22) Doi, K.; Tsutsui, M.; Ohshiro, T.; Chien, C.-C.; Zwolak, M.; Taniguchi, M.; Kawai, T.; Kawano, S.; Di Ventra, M. Nonequilibrium Ionic Response of Biased Mechanically Controllable Break Junction (MCBJ) Electrodes. *J. Phys. Chem. C* **2014**, *118*, 3758−3765.
(23) Zhang, B.; Ai, Y.; Liu, J.; Joo, S. W.; Qian, S. Polarization Effect of a Dielectric Membrane on the Ionic Current Rectification in a Conical Nanopore. *J. Phys. Chem. C* **2011**, *115*, 24951−24959.
(24) He, Y.; Tsutsui, M.; Fan, C.; Taniguchi, M.; Kawai, T. Gate Manipulation of DNA Capture into Nanopores. *ACS Nano* **2011**, *5*, 8391−8397.
(25) Newman, J.; Tiedemann, W. Porous-Electrode Theory with Battery Applications. *AlChE J.* **1975**, *21*, 25−41.

(26) Melcher, J. R.; Taylor, G. I. Electrohydrodynamics: A Review of the Role of Interfacial Shear Stresses. *Annu. Rev. Fluid. Mech.* **1969**, *1*, 111−146.
(27) Saville, D. A. Electrohydrodynamics: The Taylor−Melcher Leaky Dielectric Model. *Annu. Rev. Fluid. Mech.* **1997**, *29*, 27−64.
(28) Trau, M.; Saville, D. A.; Aksay, I. A. Assembly of Colloidal Crystals at Electrode Interfaces. *Langmuir* **1997**, *13*, 6375−6381.
(29) Ristenpart, W. D.; Aksay, I. A.; Saville, D. A. Assembly of Colloidal Aggregates by Electrohydrodynamic Flow: Kinetic Experiments and Scaling Analysis. *Phys. Rev. E* **2004**, *69*, 021405−1−021405−8.
(30) Ristenpart, W. D.; Aksay, I. A.; Saville, D. A. Electrohydrodynamic Flow around a Colloidal Particle near an Electrode with an Oscillating Potential. *J. Fluid. Mech.* **2007**, *575*, 83−109.
(31) Fuhr, G.; Schnelle, T.; Wagner, B. Travelling Wave-Driven Microfabricated Electrohydrodynamic Pumps for Liquids. *J. Micromech. Microeng.* **1994**, *4*, 217−226.
(32) Bhaumik, S. K.; Roy, R.; Chakraborty, S.; DasGupta, S. Low-Voltage Electrohydrodynamic Micropumping of Emulsions. *Sens. Actuators, B* **2014**, *193*, 288−293.
(33) Storey, B. D. Direct Numerical Simulation of Electrohydrodynamic Flow Instabilities in Microchannels. *Physica D* **2005**, *211*, 151−167.
(34) Ryu, J. C.; Park, H. J.; Park, J. K.; Kang, K. H. New Electrohydrodynamic Flow Caused by the Onsager Effect. *Phys. Rev. Lett.* **2010**, *104*, 104502−1−104502−4.
(35) Uehara, S.; Shintaku, H.; Kawano, S. Electrokinetic Flow Dynamics of Weakly Aggregated λDNA Confined in Nanochannels. *J. Fluids Eng.* **2011**, *133*, 121203−1−121203−8.
(36) Doi, K.; Uemura, T.; Kawano, S. Molecular Dynamics Study of Solvation Effect on Diffusivity Changes of DNA Fragments. *J. Mol. Model.* **2011**, *17*, 1457−1465.
(37) Doi, K.; Takeuchi, H.; Nii, R.; Akamatsu, S.; Kakizaki, T.; Kawano, S. Self-Assembly of 50 bp Poly(dA)·Poly(dT) DNA on Highly Oriented Pyrolytic Graphite via Atomic Force Microscopy Observation and Molecular Dynamics Simulation. *J. Chem. Phys.* **2013**, *139*, 085102−1−085102−10.
(38) Mei, R.; Adrian, R. J. Flow Past a Sphere with an Oscillation in the Free-Stream Velocity and Unsteady Drag at Finite Reynolds Number. *J. Fluid. Mech.* **1992**, *237*, 323−341.
(39) Mei, R. Flow Due to an Oscillating Sphere and an Expression for Unsteady Drag on the Sphere at Finite Reynolds Number. *J. Fluid. Mech.* **1994**, *270*, 133−174.
(40) Mei, R. Velocity Fidelity of Flow Tracer Particles. *Exp. Fluids* **1996**, *22*, 1−13.